Published August 1, 1976

LOW RESISTANCE JUNCTIONS IN CRAYFISH

Structural Changes with Functional Uncoupling

CAMILLO PERACCHIA and ANGELA F. DULHUNTY

From the Department of Physiology, University of Rochester, School of Medicine and Dentistry, Rochester, New York 14642. Dr. Dulhunty's present address is the New South Wales Institute of Technology, School of Life Sciences, Gore Hill, New South Wales, Australia 2065.

ABSTRACT

Electrical uncoupling of crayfish septate lateral giant axons is paralleled by structural changes in the gap junctions. The changes are characterized by a tighter aggregation of the intramembrane particles and a decrease in the overall width of the junction and the thickness of the gap. Preliminary measurements indicate also a decrease in particle diameter. The uncoupling is produced by in vitro treatment of crayfish abdominal cords either with a Ca^{++}, Mg^{++}-free solution containing EDTA, followed by return to normal saline (Van Harreveld's solution), or with Van Harreveld's solution containing dinitrophenol (DNP). The uncoupling is monitored by the intracellular recording of the electrical resistance at a septum between lateral giant axons. The junctions of the same septum are examined in thin sections; those of other ganglia of the same chain used for the electrical measurements are studied by freeze-fracture. In controls, most junctions contain a more or less regular array of particles repeating at a center to center distance of ~200 Å. The overall width of the junctions is ~200 Å and the gap thickness is 40–50 Å. Vesicles (400–700 Å in diameter) are closely apposed to the junctional membranes. In uncoupled axons, most junctions contain a hexagonal array of particles repeating at a center to center distance of 150–155 Å. The overall width of the junctions is ~180 Å and the gap thickness is 20–30 Å. These junctions are usually curved and are rarely associated with vesicles. Isolated, PTA-stained junctions, also believed to be uncoupled, display similar structural features. There are reasons to believe that the changes in structure and permeability are triggered by an increase in the intracellular free Ca^{++} concentration. Most likely, the changes in permeability are caused by conformational changes in some components of the intramembrane particles at the gap junctions.

In most vertebrate and invertebrate tissues, adjacent cells communicate directly with one another by a free exchange of small molecules. The communication occurs at gap junctions (40) or nexuses (15), structures which provide the framework for intercellular channels. In excitable cells, these channels create low resistance ionic pathways which allow electrotonic transmission of the electrical impulse (7).

In recent years, a variety of treatments have

been found to uncouple adjacent cells by reducing the permeability of the gap junctions. Two cell systems have been extensively studied in uncoupling experiments: *(a)* the epithelial cells of *Chironomus* salivary glands (23, 24, 26, 27, 39, 44–46); and *(b)* crayfish septate axons (2, 3, 28–30, 38).

In salivary glands, both the gap junctions (43) and the septate junctions (11, 43) have been examined and their structure did not appear altered by uncoupling. Gap junctions in crayfish axons have been studied, by thin sections, in various conditions of uncoupling and have been shown to be absent, in some cases (3, 28, 29), as a result of physical separation of the two membranes followed by Schwann cell invasion. In other cases, however, an increase in coupling resistance occurred without obvious alterations of the structure of gap junctions (29, 30, 38), indicating that more subtle modifications of the intercellular channels, not detectable in thin sections, may also lead to uncoupling. Recently, it has been found (8) that glutaraldehyde fixation leads to transitory uncoupling, indicating that some of the junctions observed in the electron microscope may indeed be in an uncoupled state.

An interesting hypothesis for the mechanism of uncoupling suggests that it may result from an increase in the concentration of unbound calcium in the cytoplasm (23, 46). This is based on the fact that most processes that cause an increase in coupling resistance also cause an increase in the concentration of unbound calcium. The most compelling evidence for this hypothesis has come from elegant experiments (45, 46) in which the specific calcium indicator, aequorin (48), has been used to look at the concentration of unbound calcium during phases of uncoupling in *Chironomus*. In the mammal, the calcium hypothesis has been recently supported by the uncoupling effect of intracellular injection of Ca^{++} in heart muscle cells (14).

Two relevant and curious observations were made on the structure of gap junctions in normal crayfish axons (32, 33). The center to center spacing between adjacent particles was about 200 Å in both thin sections and in freeze-fracture, but in isolated, negatively stained junctions it decreased to 150–155 Å. In lanthanum-stained preparations (32), two arrays of particles were found: in one, the particles were arranged in a fairly regular hexagonal array with a unit cell of 180–200 Å; in the other, the particles were packed more closely and less regularly at a center to center spacing as small as 125 Å. The two arrays were continuous with each other, and the closely packed ones were rarely associated with cytoplasmic vesicles. Both observations suggested interesting plastic properties in the structure of the junctions and, as a hypothesis, it was proposed that changes in the arrangement of the particles from the large to the small pattern could parallel changes in the junctional membrane permeability from low to high coupling resistance (31, 32).

To test this hypothesis, the resistance of the surface membrane and of gap junctions has been measured and the structure of the junctions has been studied in axons uncoupled by a chelator of Ca^{++} and Mg^{++} or by a metabolic inhibitor. The observations reported here indicate that electrical uncoupling is indeed paralleled by a tighter packing of the intramembrane particles. The tighter packing is accompanied by a decrease in the overall width of the junctions, in the thickness of the extracellular gap, and possibly in the diameter of the particles. Preliminary reports of these findings have been published previously (35, 36).

MATERIALS AND METHODS

Experiments were done on the ventral nerve cord of crayfish *Procambarus clarkii*. The crayfish were kept in a well-oxygenated aquarium at about 20°C. The ventral nerve cord was dissected by first removing the abdominal carapace and then sectioning the three pairs of roots to each ganglion. The roots were sectioned at a distance of about 3 mm from the ganglion. The ventral cord and ganglia could then be removed from the animal and placed in Van Harreveld's solution (51) buffered to pH 7.4 with Tris-HCl at room temperature. The cord was finally cleaned by removing the ventral artery and small fragments of muscle and connective tissue that remained attached to it. The preparation was then pinned, dorsal side up, to a Plexiglass chamber with 3 mm of Sylgard (Dow Corning Corporation, Midland, Mich.) lining the bottom. The ganglia were transilluminated and viewed by a Wild M5 Stereomicroscope. The septa cross the lateral giant axons obliquely, anteroposteriorly, and lateromedially.

Electrical Measurements

The left lateral giant axon was generally used for electrical measurements. Glass microelectrodes filled with 3 M KCl and having a tip resistance of 15–30 M were used. The arrangement of the electrodes on either side of the septum is shown in Fig. 1. A current-passing electrode was inserted on one side of the septum. A

Published August 1, 1976

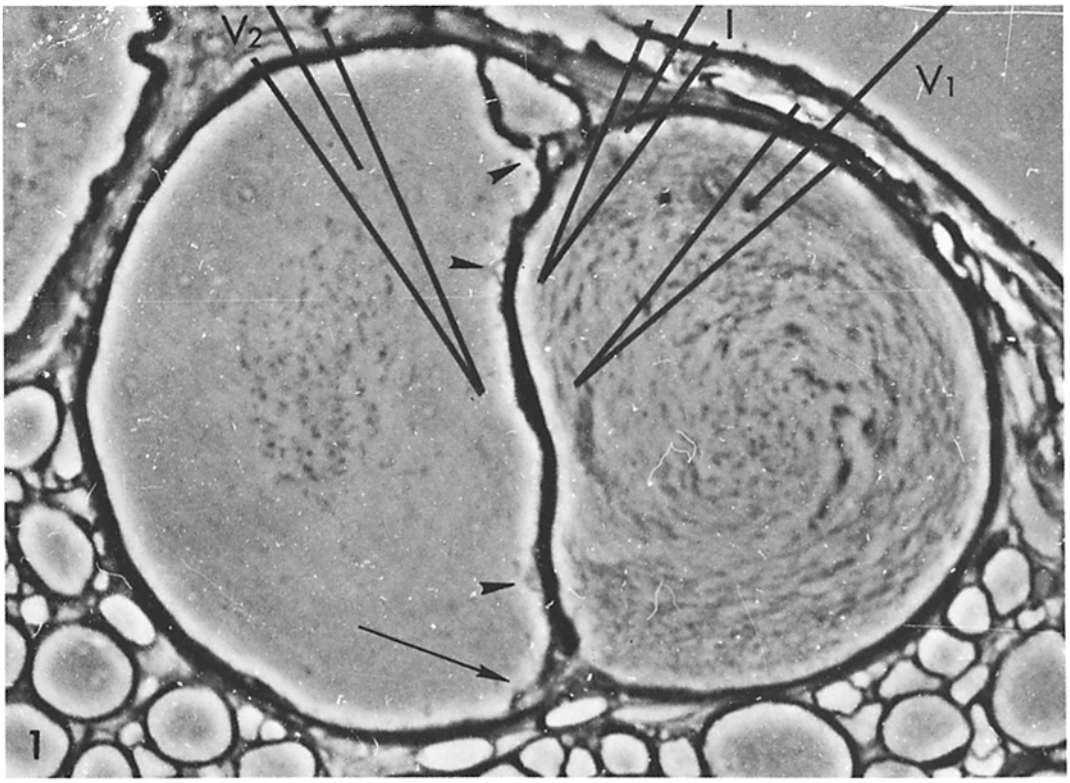

FIGURE 1 Cross section through a lateral giant axon at the septum. The axon on the right (lateral) side of the septum is the posterior and forms low resistance junctions with the anterior axon (on the left side of the septum). Most often, the junctions occur at the end of finger-like processes of the posterior axon, which find their way through the septum to reach the surface membrane of the anterior segment bulging from the septum in hemispherical protrusions (arrowheads). Occasionally, the processes can be followed all the way through the septum (arrow). For the intracellular recording, three microelectrodes were inserted in the axons; one on each side of the septum was used for recording the potential (V_1, V_2) and the third for passing current (I). × 1,000.

prejunctional voltage electrode was inserted on the same side of the septum and was used for recording prejunctional voltage changes, V_1. A postjunctional voltage electrode was inserted on the opposite side of the septum and used to record postjunctional voltage changes, V_2. The space constant of the lateral giant axons is about 2.5 mm, and the microelectrodes were inserted within a 100 μm radius of the septum. Care was taken to place the two voltage electrodes at equal distances from the current electrode.

Constant current was ensured by using a current clamp (1) and 400-ms pulses were passed every 8 s. The amplitude of the current was adjusted to give hyperpolarizations of about 20 mV. The voltage signals were fed to negative capacitance electrometers (Keithley Instruments 605, Keithley Instruments, Inc., Cleveland, Ohio) and then displayed on a Tektronix 565 oscilloscope (Tektronix, Inc., Beaverton, Ore.) and permanently recorded on Polaroid film.

Analysis of Data

The resistances calculated from the current and voltage records will be referred to as transfer resistances (17) because no attempt was made to extrapolate data to a zero electrode separation, and so we were not recording the true input resistances of the fibers. The transfer resistances $R_{x(1)}$ and $R_{x(2)}$ were calculated from V_1 and V_2 by the following relationships (6, 53):

$$R_{x(1)} = \frac{V_1}{I}, \quad (1)$$

$$R_{x(2)} = \frac{V_2}{I}, \quad (2)$$

where I is the current passed by the current clamp. These two resistances contain components of axoplasmic resistance, resistance across the surface membrane $R_{x(m)}$ and resistance across the septum $R_{x(s)}$, and

these can be obtained from the following relationships (6, 53):

$$R_{x(m)} = R_{x(1)} + R_{x(2)}, \quad (3)$$

$$R_{x(s)} = \frac{R_{x(1)}^2 - R_{x(2)}^2}{R_{x(2)}}. \quad (4)$$

The microelectrodes were allowed to settle into the axons for 30 min to 1 h after insertion and control records were taken during this period. The membrane potential increased (hyperpolarized) over this period, and both $R_{x(1)}$ and $R_{x(2)}$ also increased slightly as the membrane sealed around the microelectrodes. The absolute magnitude of $R_{x(m)}$ and $R_{x(s)}$ varied enormously from preparation to preparation. For example, $R_{x(m)}$ in the experiment illustrated in Fig. 3 was 1.6×10^5 Ω and $R_{x(s)}$ was 0.1×10^5 Ω. In the experiment illustrated in Fig. 25, $R_{x(m)}$ was 9.0×10^5 Ω and $R_{x(s)}$ was 3×10^5 Ω. The magnitude of these values must depend on the size of the axons and the architecture and number of junctions in the septum. Another factor in the value of $R_{x(s)}$ is injury, perhaps mediated by Ca^{++} leak. No attempt was made here to determine the specific resistances of the membrane or of the septum.

Treatment with Uncouplers

EDTA: One method used to prevent pH shifts during exposure to EDTA is initially to expose the tissue to Van Harreveld's solution made up without Ca^{++} or Mg^{++} (2). Thus the abdominal cords were exposed to a Ca^{++}, Mg^{++}-free Van Harreveld's solution for 10 min before exposure to 3 mM EDTA (ethylenedinitrilo tetracetate; Eastman Kodak Corp., Organic Chemicals Div., Rochester, N. Y.). Exposure to 3 mM EDTA causes an increase in coupling resistance which can be reversed by returning the preparations to normal Van Harreveld's solution. Some cords were allowed to recover in normal solution for 1–3 h.

DNP: 1,4-Dinitrophenol (DNP, British Drug Houses, Ltd., Pole, England). 0.5×10^{-3} M to 5×10^{-3} M, was dissolved in Van Harreveld's solution. Abdominal cords were transferred directly from the normal solution to the DNP solution and maintained there for several hours before fixation. No attempt to recouple these cells was made.

The preparations were fixed for electron microscopy (see below) at desired times during the treatments. All experiments were done at room temperature (i.e. approximately 25°C). The pH of all solutions was adjusted to 7.4 immediately before use.

Electron Microscopy

The abdominal cords were fixed for 2 h at room temperature by immersion in a 3% glutaraldehyde-H_2O_2 solution (37) buffered to pH 7.4 with 0.1 M Na^+ cacodylate and washed for 1 h in 0.2 M buffer. The ganglion on which the intracellular recordings were made was postfixed for 2 h at room temperature in a solution containing 2% OsO_4 and 1% lanthanum buffered to pH 7.4 with 0.1 M cacodylate buffer prepared by mixing 1:1 a 4% OsO_4 solution in 0.2 M cacodylate buffer with a 2% lanthanum solution taken to pH 7.6 with 0.1 N NaOH. The lanthanum acted here as a positive stain enhancing the electron opacity of the membranes and allowing one to distinguish more clearly the intramembrane particles at the junction. Dehydration was carried out in graded alcohols and embedding was in Epon. Thick sections (~2 μm thick) were cut serially through the ganglia with an LKB Ultrotome microtome along planes normal to the long axis of the abdominal cord, and observed by phase-contrast microscopy to localize that septum, between lateral giant fibers, where the electrical recordings were made. Thin sections (~500 Å thick) were cut from areas of the septum rich in junctions and collected on uncoated 400-mesh grids. The sections were stained by immersion for 15 min in a saturated solution of uranyl acetate in 50% ethanol, followed by a 3-min immersion in a 3% solution of lead salts (47).

The other ganglia of the same abdominal cord were prepared for freeze-fracture in the following way. After fixation in glutaraldehyde, they were immersed in a 5%, 10%, 20%, 30% series of glycerol solutions in H_2O at 30-min to 1-h intervals at room temperature. Each ganglion was mounted on an aluminum holder, rapidly frozen in liquid Freon 22 (Virginia Chemical Inc., Portsmouth, Va.) to ~−150°C, and transferred to a Denton freeze-fracture device (Denton Vacuum Inc., Cherry Hill, N. J.) mounted on a Kinney (KSE-2A-M) evaporator (Kinney Vacuum Co., Boston, Mass.). The freeze-fracture device was modified for platinum evaporation by adapting a Fullam electrode (Ernest F. Fullam, Inc., Schenectady, N. Y.) in place of the Denton electrode. The shroud and the specimen holder were previously cooled with liquid nitrogen. The ganglia were cross-fractured at ~−110°C and immediately shadowed with carbon-platinum at 45°C followed by carbon at 90°C. All replicas were made at a vacuum of $\sim 5 \times 10^{-7}$ torr. The carbon-platinum electrode was out-gassed before each experiment by passing a current of about 25 A through it for 30–60 min. After carbon evaporation, dry nitrogen was introduced into the bell jar and the replicas were immediately coated with a drop of 2% collodion in amyl acetate (34). The specimens were digested in Chlorox and the collodion-coated replicas, washed three times in distilled water, were collected on 400-mesh grids. The collodion film was dissolved by immersion in amyl acetate for 2–3 min.

Control abdominal cords were treated with colloidal lanthanum as extracellular tracer (41) as follows: some specimens were treated by a lanthanum-NaCl solution for 5 min to 2 h followed by a 2-h fixation in 3% glutaraldehyde (pH 7.4) containing 1% lanthanum and a 2-h postfixation in 2% OsO_4 (pH 7.4) containing 1% lanthanum. Other specimens were fixed directly in glu-

Published August 1, 1976

taraldehyde-lanthanum without pretreatment with the lanthanum-NaCl solutions. The lanthanum-NaCl solution was prepared by vigorously stirring 25 ml of a 4% lanthanum nitrate solution while adding 0.1 M NaOH so that the pH came to 8 within 3–4 min. Normally, addition of 20–25 ml of NaOH was necessary. The final solution was crystal clear. NaCl was added to reach the final osmolarity of 436 mosM (osmolarity of crayfish blood) (51). Dehydration and embedding were carried out as previously described.

All specimens were examined with an AEI EM 801 electron microscope. The microscope magnification was standardized before each photographic exposure by eliminating the hysteresis of the lenses. All magnifications were previously standardized with a carbon grating replica (No. 1002, Ernest F. Fullam Inc.). In all the freeze-fracture micrographs, the direction of the platinum shadowing is from bottom up. The fracture faces have been labeled according to a recently revised nomenclature (10): thus, P indicates the fracture face of the protoplasmic leaflet and E that of the exoplasmic leaflet.

Measurements of Particle Spacings

In sections, only those junctional regions which appeared precisely cross-sectioned and displayed a sharp beaded profile were selected. The length (in Angstroms) of the beaded profile was measured and divided by the number of beads (minus one) to average the spacings between adjacent beads. Sharp beaded profiles result from the precise superimposition of adjacent particles which occurs when the plane of section runs precisely perpendicular to rows of particles. In this case, the average spacing between beads represents the spacing between parallel rows of particles; such spacing, assuming a regular hexagonal pattern, is 86.6% of the center to center spacing between adjacent particles.

In freeze-fracture, the center to center distance between adjacent particles was measured. Only interneuronal junctions were selected. In junctions containing particles not regularly packed, the center to center distance between most of the adjacent particles was measured and the average value was calculated. In junctions containing regular hexagonal arrays, the average center to center distance was obtained by calculating the particle periodicity along each of three rows of particles oriented at 120° to each other and by making a final average of the three means. Due to the wavy course of the fracture plane, some junctions may be slightly tilted when photographed in the electron microscope. The tilting, of course, will introduce errors in the measurement of particle periodicity; however, since both the control and the treated junctions are subjected to the same artifacts, the errors tend to cancel out. All measurements were performed on micrographs of junctions enlarged × 123,600 using a × 7 measuring magnifier (Bausch & Lomb, Inc., Rochester, N. Y.) equipped with a 20-mm long scale calibrated to a minimum separation of 0.1 mm (in the micrographs 0.1 mm = 8.09 Å).

OBSERVATIONS

Control Junctions

Control axoaxonal junctions appear, in section, as regions of close apposition between two adjacent axons. In cross sections, the profile of the junctions is beaded because of the presence of intramembrane particles which protrude from the membrane surface and are in register with the particles of the adjoining membrane (Fig. 5). The junction is 320–340-Å thick in the region of the particles and ~200-Å thick between particles. The gap between the apposing membranes is 40–50 Å and membranes on both sides of the junction have one or more layers of 400–700-Å vesicles associated with them.

In freeze-fracture the junctional membranes split. Most of the particles remain attached to the external leaflet (face E, Fig. 11), but a few are seen on the cytoplasmic leaflet (face P, Fig. 2). Most commonly, the particles are not packed in a regular pattern but they can occasionally be seen in a slightly distorted hexagonal array when they appear in tangential sections or on face P of the fractured membranes (Fig. 2).

In sections, the average center to center distance between adjacent beads is 205 Å (Fig. 5) (this, presumably, is the average spacing between rows of particles; see Materials and Methods). In freeze-fracture, most junctions contain particles at an average center to center distance of 200 Å (Figs. 2, 11). Interestingly, in isolated, negatively stained junctions the particles are organized in a regular hexagonal array at a center to center distance of 150–155 Å (see *inset*, Fig. 2).

Uncoupling by EDTA

The sequence of solution changes was: normal Van Harreveld's solution to Ca^{++}, Mg^{++}-free Van Harreveld's solution for 10 min; Ca^{++}, Mg^{++}-free Van Harreveld's with 3 mM EDTA for 1 h; return to normal Van Harreveld's solution for 1–3 h. Fig. 3 illustrates the changes in coupling resistance $R_{x(s)}$ and membrane resistance $R_{x(m)}$ during these solution changes. Within 45 min to 1 h of exposure to EDTA, the coupling resistance increased to a maximum (see the filled circles and broken line in Fig. 3). The magnitude of the increase in coupling resistance varied from preparation to preparation, and we observed a range of changes from 2 to 15 times the control resistance. The membrane resistance (see open circles and solid line in Fig. 3) falls to 10% to 50% of the control resistance within 10

Published August 1, 1976

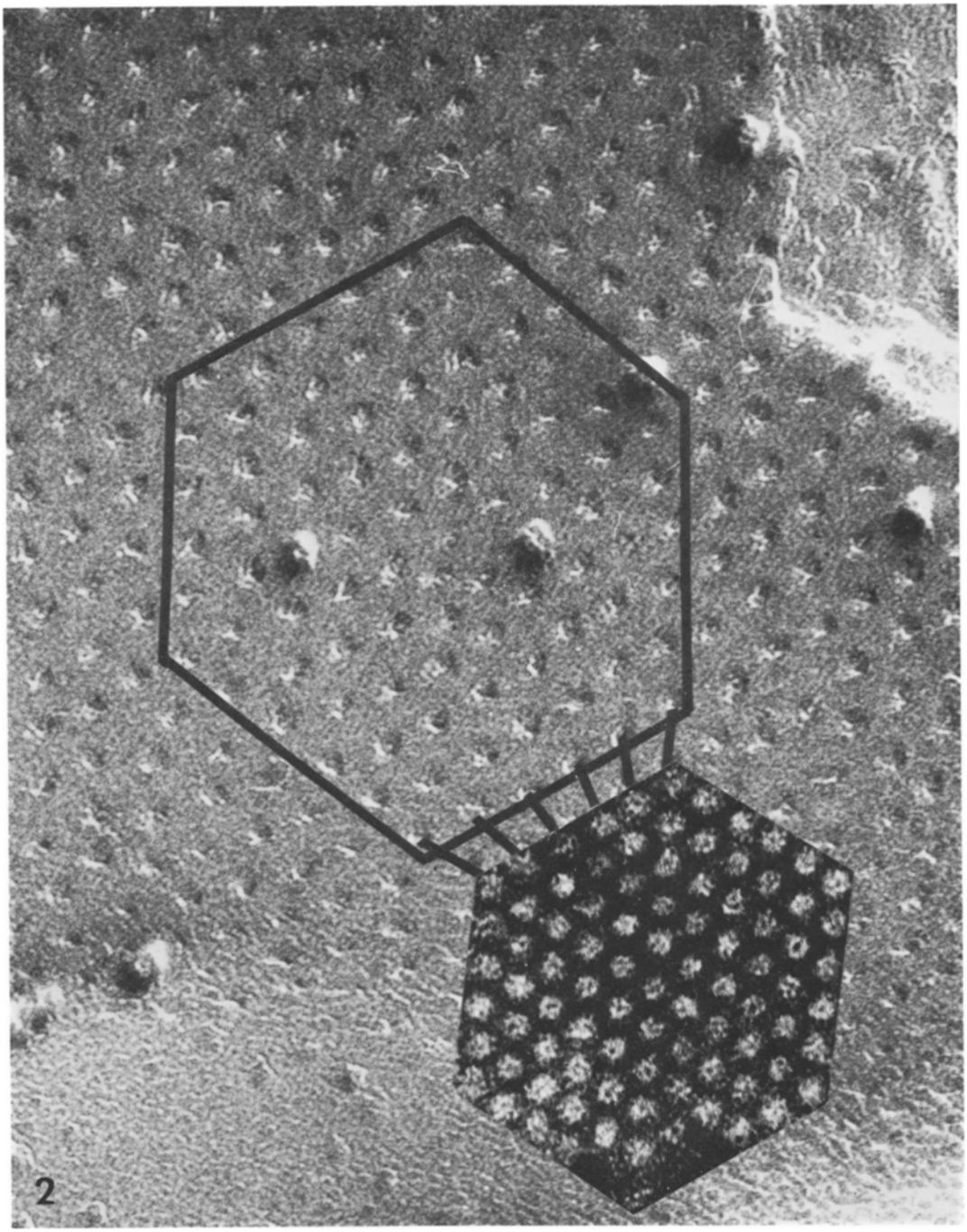

FIGURE 2 Comparison between freeze-fracture and negative staining of junctions from control preparations. Face P of a fractured junction is shown. Most of the particles have been fractured away with the external membrane leaflet, leaving a fairly regular hexagonal array of pits. A few pits are occupied by particles. The inset shows a fragment of an isolated, PTA negatively-stained junction. Interestingly, the unit cell dimension of the arrays is ~200 Å in the freeze-fractured junction, 150–155 Å in the negatively stained one. Notice the difference between the two hexagonal areas which contain the same number of particles at the same magnification. × 420,000.

Published August 1, 1976

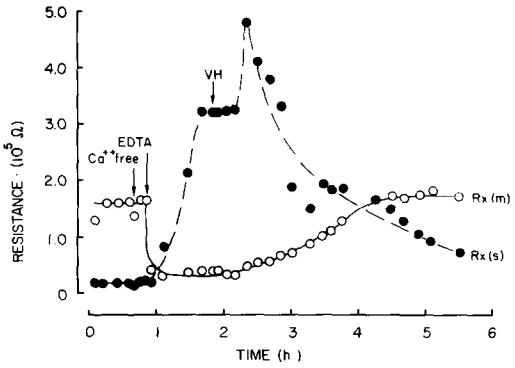

FIGURE 3 Time course of septal resistance $R_{x(s)}$ (filled circles) and membrane resistance $R_{x(m)}$ (open circles) during treatment with a Ca^{++} chelator (EDTA) followed by Van Harreveld's saline (VH). EDTA treatment is preceded by a brief treatment with Ca^{++}, Mg^{++}-free solution. In EDTA, $R_{x(s)}$ increases. Upon return to VH $R_{x(s)}$ increases further, then decreases rapidly to control values. Simultaneously, $R_{x(m)}$ decreases and then increases to control values.

min of exposure to EDTA but does not decrease further during longer exposure. The reduction in membrane resistance is paralleled by a significant reduction in the membrane potential (depolarization). Upon return to normal Van Harreveld's solution, the coupling resistance initially increased further, possibly because of Ca^{++} influx from the surface membrane, going to values as great as 30 times control, and reached a maximum within 30 min to 1 h of changing the solution. The coupling resistance then fell continuously over 1–2 h until it had returned to near its control value. The membrane resistance returned slowly to normal in Van Harreveld's solution and was followed by a recovery of membrane potential. When experiments were taken through to full recovery (as illustrated in Fig. 3), the membrane potential recovered to −85 mV, when the electrodes were removed from the axons.

Sections

Thin sections were cut through the same septum on which electrical measurements had been made. When the coupling resistance was high (from 9.5 to 30 times the control values), the center to center distance between adjacent particles was significantly reduced (Fig. 6, 8), and when the junctions were recoupled the center to center distance between the particles returned to its normal value (Fig. 7). In high resistance septa, more than 60% of the length of junctional profiles contains beads with center to center distances less than 170 Å (see Fig. 4). The center to center distances in control septa and recoupled septa were greater. In control septa, 86% of the junctional profile contains beads with center to center distances of 200–210 Å, and in recoupled septa 68% of the junctional profile contains beads with center to center distances of 200–210 Å.

When the repeat is less than 170 Å, the individual particles cannot be easily identified in positively stained sections (see Fig. 8) but are quite clear in junctions treated by lanthanum-NaCl solutions before fixation, as illustrated in Fig. 9. These junctions differ from control junctions in other features. In particular, the thickness of the junction is about 180 Å compared to 200 Å in control, and the gap is 20–30 Å compared to 40–50 Å in control preparations. In addition, the number of vesicles associated with the junctional regions appears reduced, as illustrated in Figs. 8, 9, and 27.

Freeze-Fracture

In each experiment, two or three of the remaining five abdominal ganglia (usually the second, third, and fifth ganglia) were prepared for freeze-fracture. Only interneuronal junctions were photographed. Gap junctions between neurons are easily distinguishable from those between glial cells because in the latter the particles are smaller and are always aggregated in a completely irregular fashion on both P and E faces. In addition, the junctions can be identified on the basis of the structural differences between neuronal and glial membranes. As previously published, only neuronal membranes contain chains of ~80-Å particles fairly regularly packed in a rhomboidal pattern (34), and only glial membranes contain circular dimples (on face P), complementary images of conical protrusions on Face E, which correspond to the mouth of tubular invaginations of the surface membrane which form the tubular lattice (34). Most of the junctions studied are between neuronal processes of medium and small size which interact with each other at the neuropile. These junctions are roughly circular and measure 0.1–1 μm in diameter.

When frequency histograms of the center to center distances are plotted, as in Fig. 10, the junctions appear to be distributed over a range from 140 Å to 219 Å. For convenience, we have defined four groups, those with a 200–219-Å separation, those with a 180–199-Å separation, those

Published August 1, 1976

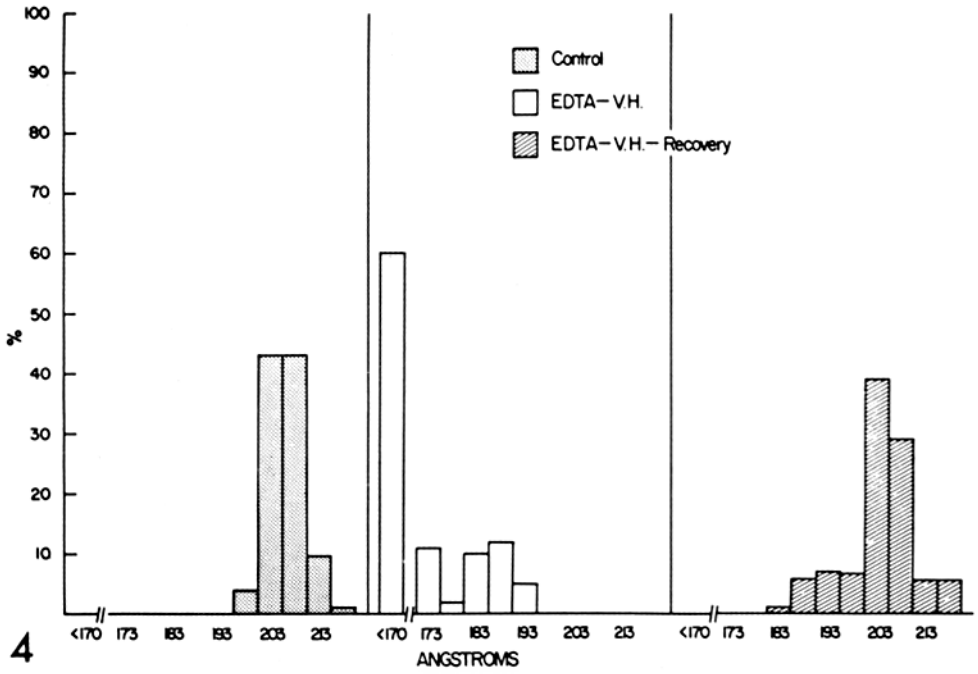

4

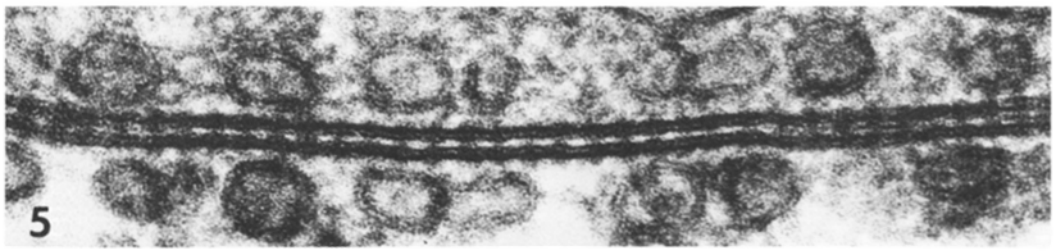

5

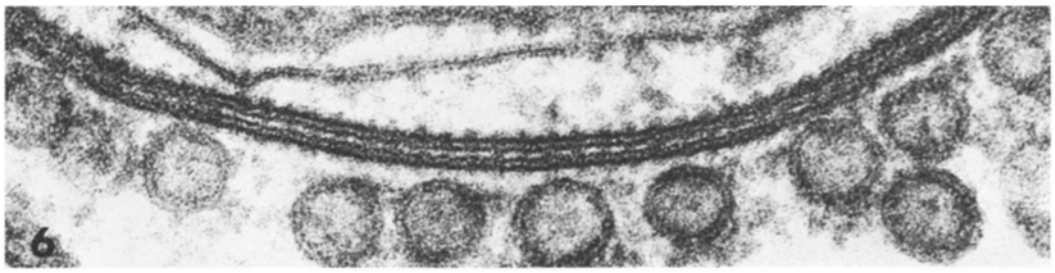

6

7

Published August 1, 1976

with a 160–179-Å separation, and those with a 140–159-Å separation. The regularity of packing appears to increase with decreases in the unit cell size. In the 200–219-Å group, the junctions contain particles packed quite irregularly, most often at a center to center distance of 200–205 Å (Figs. 11, 14, 15). In the 180–199-Å group, the packing is more regular and most often the average particle repeat is 180–185 Å (Figs. 16, 17). In the 160–179-Å group, most junctions contain a regular hexagonal array of particles with a unit cell of 170–175 Å (Figs. 18, 19). In the 140–159-Å group, most junctions contain a fairy regular hexagonal array of particles with a unit cell of 150–155 Å and often the membranes appear to be sharply curved (Figs. 12, 20, 21–24). In freeze-fracture, the sharp curves appear as convexities or concavities of the fracture surface. Convexities (see Figs. 12, 20, 22, and 24) are more common on the E faces than are concavities (Fig. 23). This, however, does not mean that convexities correspond to junctions whose membranes have separated, since in steplike fractures as well as in cross sections the integrity of the junctions was always apparent.

The size of individual junctional particles varies a great deal in freeze-fracture preparations due to variable contamination and/or replica thickness in different replicas and different regions of the same replica. It is therefore impossible to obtain absolute measurements of particle diameter in freeze-fracture. However, it is possible to gain information on relative changes in particle diameter if the measurements are made on nearby areas of the same replica, oriented similarly with respect to the shadowing source. In treated ganglia, usually all junctions belonging to the same cell have similar packing arrangement. In some rare cases, however, we have seen nearby junctions of the same cell with different packing arrangement. Fig. 24 shows one such case, in which a typical junction with particles at 150–155-Å separation is close to two junctions with particles at ~200 Å separation. Such cases offer a good opportunity for comparing particle diameter between the junctions which are more common in controls (200–205-Å separation) and those more common in treated ganglia (150–155-Å separation). In Fig. 24, the size of individual particles was measured in a direction normal to the direction of platinum shadowing, and the average particle size was 152 ± 9.7 Å (mean ± 1 SD) in the two ~200-Å junctions and 121 ± 12.5 Å (mean ± 1 SD) in the 150–155-Å junctions.

In negatively stained junctions (see *inset*, Fig. 2), the unit cell dimensions are 150–155 Å. It is

FIGURE 4 Histogram of frequencies (in percentiles) of center to center distances between adjacent beads measured on cross-sectional profiles of junctional membranes at the septa where the intracellular recordings were made. Left: control junctions. Center: junctions fixed at the highest $R_{x(s)}$ values (from 9.5 to 30 times the control values), after return to Van Harreveld's saline (VH), after EDTA treatment. Right: junctions fixed when a more or less complete recovery of control $R_{x(s)}$ values was obtained. A representative record of the time course of changes in $R_{x(s)}$ is shown in Fig. 3. A total length of 39.05 μm of cross-sectional profile was measured (control = 7.89 μm; EDTA-VH = 8.99 μm; recovery = 22.17 μm).

FIGURE 5 Cross-sectional profile of a control junction from a septum between lateral giant fibers. The membranes show a beaded profile due to rows of intramembrane particles which are in register and protrude from both membrane surfaces. The beads repeat every ~210 Å. The overall width of the junction is 320–340 Å at the beads, ~200 Å between beads. The gap measures 40–50 Å. 400–700-Å vesicles lie in layers close to both cytoplasmic surfaces of the junction. × 200,000.

FIGURE 6 Cross-sectional profile of a junction from a septum between lateral giant fibers treated with EDTA followed by Van Harreveld's saline. The septum was fixed in uncoupled conditions, i.e. at the highest $R_{x(s)}$ values (see Fig. 3). The average center to center distance between beads is ~170 Å. Notice that the concave side of the junction is not coated with vesicles, while normal 400–700-Å vesicles lie close to the convex side. × 200,000.

FIGURE 7 Cross-sectional profile of a junction from a septum between lateral giant fibers treated by EDTA followed by Van Harreveld's solution. The septum was fixed after complete recovery of electrical coupling, i.e. when $R_{x(s)}$ had decreased back to control values (see Fig. 3). The average center to center distance between adjacent beads is ~216 Å. × 200,000.

Published August 1, 1976

FIGURE 8 Cross-sectional profile of a junction from a septum of a lateral giant fiber fixed in uncoupled conditions, as the junction of Fig. 6. In most of the junctional profile (right of center) the beads are not visible, the average width of the junction is ~180 Å (control ~200 Å), and the gap measures 20–30 Å (control 40–50 Å). The junction is sharply curved and is associated with only a few scattered vesicles. The arrows point to a region which is precisely cross sectioned. × 169,000.

FIGURE 9 Section through a junction from a septum of a lateral giant fiber treated with lanthanum hydroxide before and during fixation. This junctional region is similar to the one shown in Fig. 8; here, also, the overall width of the junction is ~180 Å. The junction is sharply curved and is associated with only a few vesicles. Because of the lanthanum precipitated in the gap, the particles are negatively stained. Where the junction is cut tangentially, the average center to center distance between adjacent particles is ~150 Å. The arrowheads point to the lanthanum-filled spaces between adjacent pairs of particles. × 169,000.

reasonable to assume that these correspond to the 150–155 Å junctions seen in freeze-fracture (Fig. 12) and to those regions which do not show particle periodicity in thin sections (Figs. 8, 9). In all types of junctions, some particles can be found with a central depression on either their cytoplasmic or their extracellular side.

Freeze-fracture of ganglia neighboring those used for electrical measurements (see Materials and Methods) show that in control preparations 83% of the junctions have center to center distances greater than 180 Å (Figs. 10, 11). If the ganglia are fixed after 60–90 min in Van Harreveld's solution, after EDTA exposure, i.e. when the coupling resistance reaches the highest values, 34% of the junctions have distances greater than 180 Å, the majority of the remaining 66% being in the 140–159-Å group. If the ganglia are fixed after recovery of the coupling resistance, i.e. 3–4 h after return to normal solution, 79% of the junctions have an average center to center distance greater than 180 Å (Figs. 10 and 13). The structural appearance of the recoupled junctions is thus very similar to that of the control preparations.

Uncoupling by DNP

The effects of exposure to DNP solution (0.5×10^{-3} to 5×10^{-3} M DNP in Van Harreveld's solution) on the coupling and membrane resistances are illustrated in Fig. 25. The coupling re-

Published August 1, 1976

sistance starts to increase almost immediately after exposure to DNP and reaches a maximum, along an S-shaped curve, in 10–15 min of exposure. The coupling resistance can increase to eight times its control value in this solution. The membrane resistance quickly falls to 30% of its control value, and this change is accompanied by significant depolarization of the membrane potential.

Sections

Sections through the septa on which the electrical measurements were made show that in almost 60% (Fig. 26) of the junctional profiles the beads repeat with average center to center distances less than 170 Å, while in controls 86% (Fig. 26) of the profiles show beads repeating at 200–210 Å. In junctions with <170-Å repeat, the thickness of the junction and the size of the gap are less than in control preparations; the junctions do not display particle profiles in thin sections and are rarely associated with cytoplasmic vesicles (Fig. 27). Occasionally, the small junctions can be seen to be continuous with areas of normal junctional profile (Fig. 27).

Freeze-Fracture

In replicas of ganglia treated with DNP, 74% of the junctions have particles at a center to center distance of 140–159 Å (Figs. 28, 29) compared to control junctions where 83% have particles at a center to center distance greater than 180 Å. The reduction in particle spacing is accompanied by curvature of the junctional membranes (Figs. 28, 29). In some preparations, the nonjunctional membranes are slightly wavy and aggregates of nonjunctional particles are seen (Figs. 28, 29). It is interesting to note that the particle-free areas resulting from the aggregation of random particles appear to match similar areas in adjacent cells (see Fig. 29). This may be evidence for interaction of random particles from adjacent cells across the intercellular space. A similar phenomenon has been observed in myelin lamellae by R. G. Miller of the University of California, San Diego (personal communication).

DISCUSSION

The experiments described in this paper show a relationship between structural changes and electrical uncoupling of gap junctions in crayfish axons. In addition, reversibility of the electrophysiological changes was accompanied by reversibility of the structural changes.

Preparations treated with DNP showed a rapid and sustained increase in coupling resistance. Both sections of septa used for electrical measurements and freeze-fracture of other septa in the ganglion show a significant reduction in the center to center distances between particles. Treatment with EDTA followed by Van Harreveld's solution resulted in a transient increase in coupling resistance and then a slow but more or less complete recovery over several hours.

Both the time course of the transient increase and the time course of recovery were very variable. Correlation between electrical coupling and particle separation was good in both EDTA-VH and DNP experiments when sections of the septum used to measure coupling resistance were studied. A less precise correlation was found with particle separation in freeze fractures of junctions from neighboring ganglia in EDTA-VH experiments. This can be explained by the variability in the time course of changes in coupling resistance in different neurons, and by delays in diffusion of both physiological agents and fixative to different regions of the ganglia.

Interesting structural changes are associated with tight packing (center to center distances of less than 170 Å). They include: *(a)* a decrease in the total junctional width; *(b)* a decrease in the thickness of the extracellular gap; and *(c)* a possible decrease in particle size. The reduction in gap size and overall junctional thickness may be due to changes in particle size. In control junctions, the 40–50-Å gap is set by matching particles which protrude from each membrane for 20–25 Å. Therefore, a reduction in the gap width to 20–30 Å implies that the particles protrude for only 10–15 Å, possibly because of a decrease in the length of the particles or a slight flattening of their extracellular end. In both cases, the length of the particles entering the gap and, consequently, the thickness of the gap would be reduced. This possibility may be supported by recent data on isolated liver gap junctions studied by X-ray diffraction (D. L. D. Caspar, Brandeis University, Waltham, Mass.; personal communication).

It is possible that the decrease in particle size reflects conformational changes which reduce the conductivity of the ionic channels. The hypothesis of conformational changes may be supported by the fact that the particles cannot be easily distinguished in positively stained sections of tightly

Published August 1, 1976

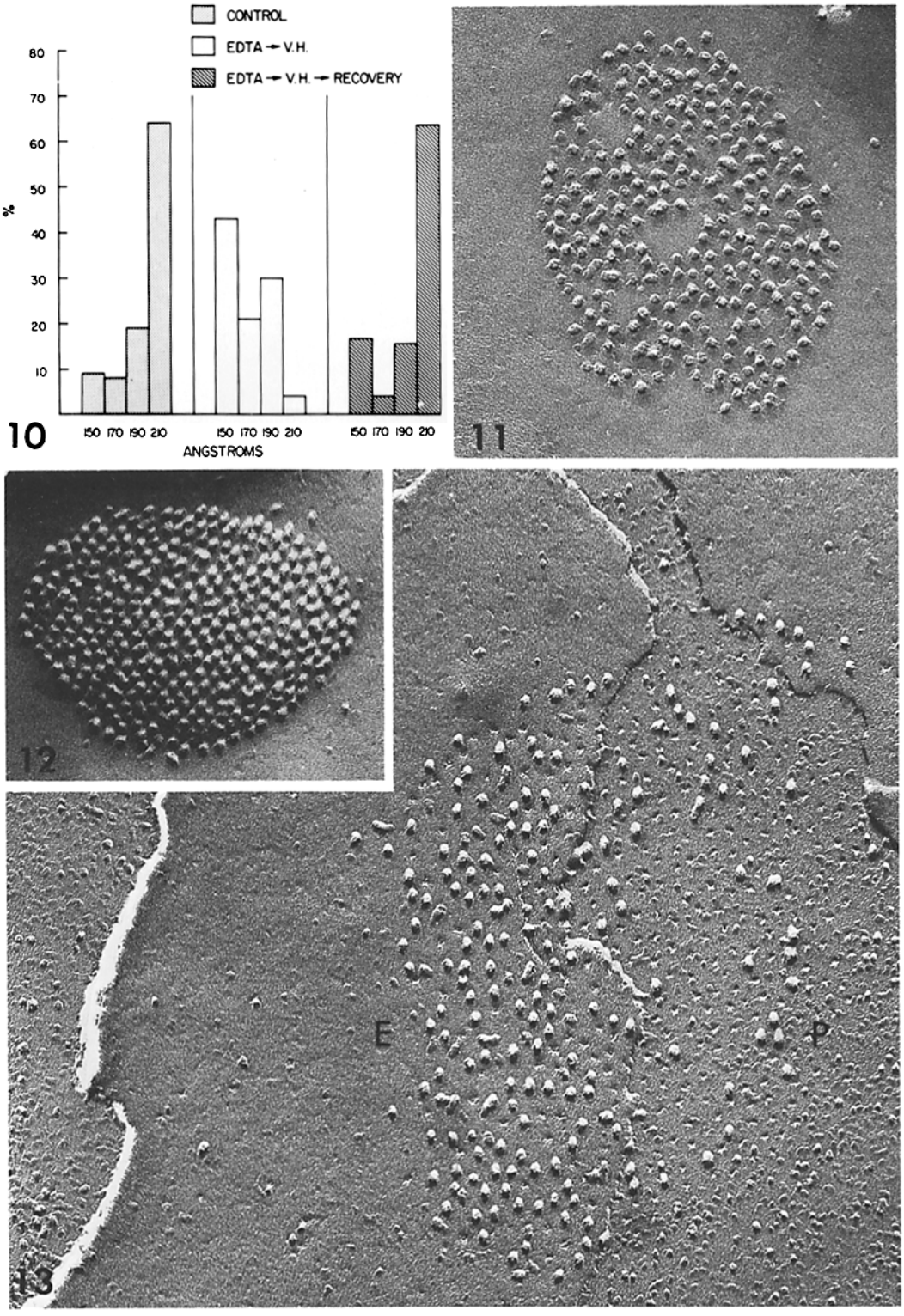

Published August 1, 1976

packed junctions. This might be explained if protein conformational changes decrease the affinity of the particle for osmium and/or other metal stains used.

Intracellular vesicles appear to be almost absent in the vicinity of tightly packed junctions. The function of the intracellular vesicles is still obscure. Keeter et al. (22) and Peracchia (unpublished observations) have observed vesicles only on the presynaptic side of rectifying low resistance junctions. D. D. Potter (personal communication) has suggested that the vesicles may be Ca^{++}-sequestering organelles. Ca^{++} enters axons during action potential activity (5, 21), and an increase in free intracellular Ca^{++} may block transmission (see below). There must, therefore, be an efficient Ca^{++}-sequestering system in the region of the junction, and the vesicles may contain this system. Since there are no vesicles on the postsynaptic side, rectification could be due to a higher concentration of unbound Ca^{++} on one side of the junction.

The intracellular concentration of unbound calcium is increased by treatment with DNP and by treatment with EDTA followed by normal Van Harreveld's solution. If the vesicles are sensitive to Ca^{++} concentration, they may be damaged by continued exposure to high Ca^{++} concentration.

Curiously, the membranes of junctions with particle separation of 150–155 Å are sharply curved, giving the freeze-fractured junctions an appearance of domes or concavities. It is possible that the process of particle aggregation and/or recovery proceeds independently in the two axons. At one time, the particles are aggregating or disaggregating, shrinking or swelling in just one of the two membranes, and consequently deforming the junctional appearance as described.

It is interesting that sharply curved junctions have vesicles only on the convex surface (Fig. 6). The uncoupling process may start on the concave side of the junction and trigger both the disappearance of the vesicles and aggregation of the particles on that side.

In a previous work (33) it has been suggested that the 25-Å depression at the center of both the cytoplasmic and the extracellular end of the particles could represent the internal and the external mouth of the ionic channel. Therefore, one may wonder why the particles still show central depressions in closely packed junctions despite the reduced ionic conductance. The channels may be

FIGURE 10 Histogram of frequencies (in percentiles) of average particle periodicity in freeze-fractured junctions from ganglia neighboring the ones in which the electrical measurements were made. Left: control junctions. Center: junctions treated with EDTA followed by Van Harreveld's saline and fixed when the highest $R_{x(s)}$ values (9.5–30 times control values) were measured at a septum. Right: junctions treated with EDTA followed by Van Harreveld's saline and fixed after recovery of control $R_{x(s)}$ values was obtained. The time course of $R_{x(s)}$ is shown in Fig. 3. 279 junctions were measured (control = 81; EDTA-VH = 135; recovery = 63).

FIGURE 11 Freeze-fracture replica of a control junction (face E). The particles are aggregated irregularly at a center to center distance of 190–200 Å. Notice that the junction lies flat. × 142,000.

FIGURE 12 Freeze-fracture replica of a junction (face E) from a ganglion treated with EDTA followed by Van Harreveld's solution and fixed when the highest values of $R_{x(s)}$ were measured at a septum (see Fig. 3). The particles form a fairly regular hexagonal array, and their average center to center distance has decreased with respect to controls to 150–155 Å. Notice that the junction is curved, displaying a convex, domelike shape. This junction has the same particle periodicity as isolated, PTA-stained junctions (Fig. 2, *inset*). × 142,000.

FIGURE 13 Freeze-fracture replica of a junction (fractured in a steplike fashion) from a ganglion treated with EDTA followed by Van Harreveld's saline and fixed after recovery of the electrical coupling, i.e. when the $R_{x(s)}$ of a septum had decreased to control values (see Fig. 3). As in most control junctions, the particles form an irregular array and repeat (in this junction) at a center to center distance of 200–210 Å. Notice that the fracture plane steps, at the junction, from one cell to the other, thus exposing the face E (*E*) of one membrane and the face P (*P*) of its adjacent membrane. In this junction, an unusually high number of particles fracture with the cytoplasmic leaflet, leaving pits on Face E. This, however, is not a feature characteristic of recoupled junctions. × 142,000.

Published August 1, 1976

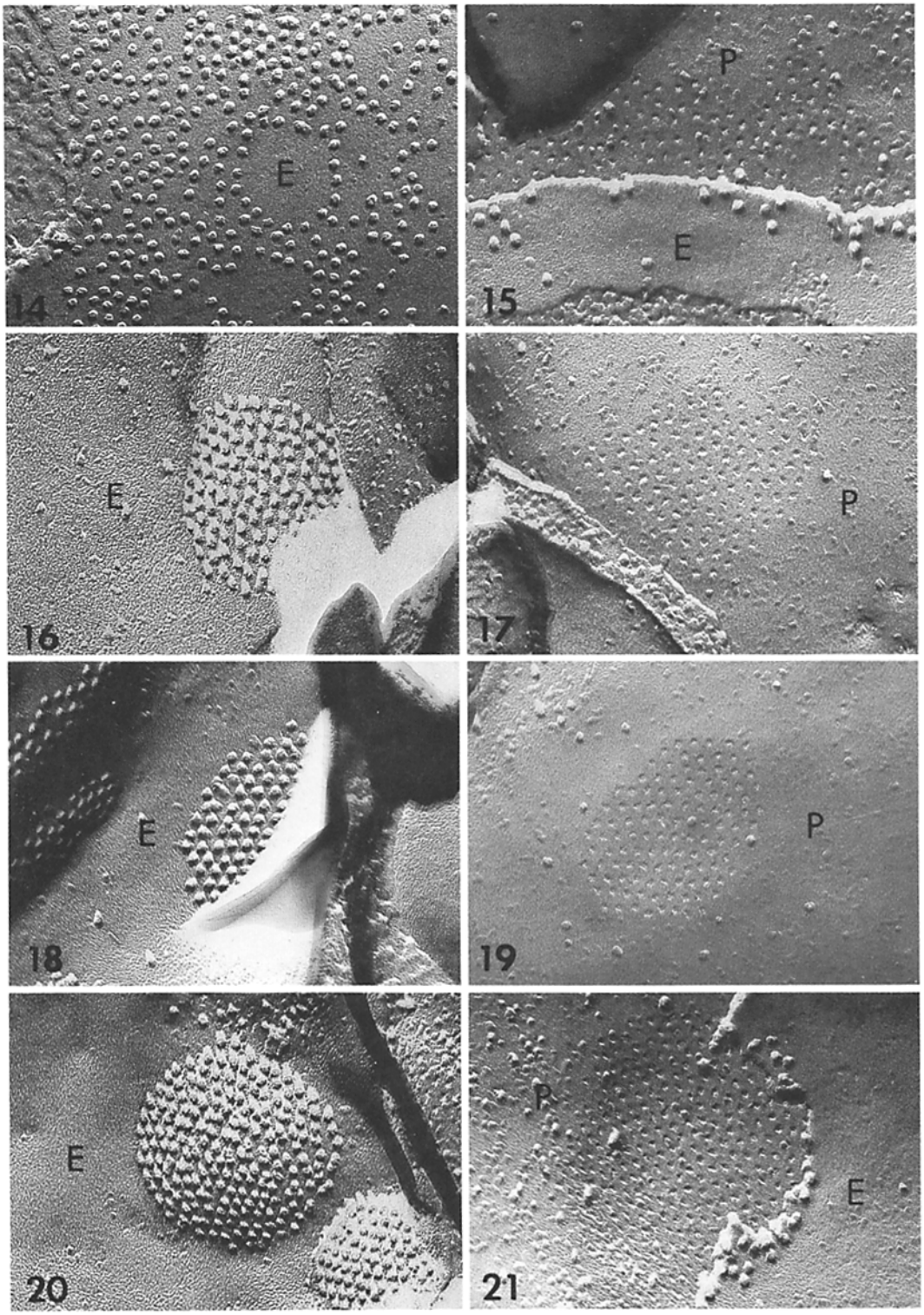

blocked in deeper regions without affecting the superficial depressions. Alternatively, the occlusion of the channels may take place in discrete regions of either the cytoplasmic or the extracellular surface of the particles which may not be exposed by freeze fracture.

In both EDTA and DNP experiments, an increase in unbound intracellular Ca^{++} concentration is likely to cause electrical uncoupling and the structural change at the junctions. Functional uncoupling and structural changes will be discussed separately because, although we believe that the changes in junctional permeability are produced by the changes in the structure of the junctions, it is still possible that the two events are simply parallel phenomena.

The concentration of unbound Ca^{++} increases as a result of Na^{+} influx when cells are exposed to solutions which do not contain either Ca^{++} or Mg^{++} (4, 13). The metabolic inhibition caused by DNP could release Ca^{++} from mitochondria (9, 12, 16, 18, 52) and increase Ca^{++} influx across the surface membrane (25). In both cases, increases in unbound intracellular Ca^{++} have been directly demonstrated with aequorin (45, 46). Changes in coupling resistance have been shown to parallel changes in unbound Ca^{++} concentrations (46).

The evidence that the increase in unbound intracellular Ca^{++} is responsible for structural changes of the junctions is indirect. Isolated, negatively stained junctions are likely to be uncoupled because *(a)* they contain particle arrays with a unit cell of ~150 Å, which corresponds to the particle separation in junctions of axons uncoupled by EDTA-VH or DNP, and *(b)* because the mechanical injury with homogenization would lead to uncoupling (2, 27) due to Ca^{++} influx through the damaged surface membrane (27). Removal of Ca^{++} from the isolated junctions should result in a recovery of the control values of particle periodicity. This may be the case in axodendritic gap junctions of goldfish brain. In goldfish (42) as well as in many other vertebrates (50), the unit cell dimension of the junctions is 95–100 Å in junctions fixed in the intact tissue, but it decreases to ~85 Å in isolated junctions. A control dimension of about 100 Å was obtained by treating the isolated junctions with EGTA (54). However, the authors did not interpret this change as a recovery of normal junctional structure but rather as an early step of junctional breakdown (54).

It is interesting that glutaraldehyde also increases, although transitorily, the coupling resistance in crayfish septate axons and other cells (7, 8), so that glutaraldehyde-fixed junctions may be in the uncoupled state regardless of treatment before fixation. The increase in coupling resistance caused by glutaraldehyde probably follows a reaction between the fixative and specific groups at or close to the channels. It is well known that glutaraldehyde does not cause muscle contracture, indicating that intracellular Ca^{++} is not increased by fixation. Moreover, structural changes were seen in the uncoupled junction either fixed *in situ* or isolated unfixed (negative staining), indicating that the changes are independent from fixation. In addition, the uncoupling effect of glutaraldehyde is transitory since after a few minutes of fixation

FIGURES 14–21 Freeze-fracture replicas of four most representative junction types. The junctions of Figs. 14 and 15 are from control ganglia; the others are from ganglia treated as described in the legend to Fig. 12. *E* = face E; *P* = face P. × 134,000.

FIGURES 14 and 15 Most common junctions of the 200–219-Å group. Particles and pits are irregularly packed at an average center to center distance of 200–205 Å.

FIGURES 16 and 17 Most common junctions of the 180–199-Å group. Particles and pits form a fairly regular array and repeat at an average center to center distance of 180–185 Å.

FIGURES 18 and 19 Most common junctions of the 160–179-Å group. The particles and pits form a very regular hexagonal array with a unit cell of 170–175 Å.

FIGURES 20 and 21 Most common junctions of the 140–159-Å group. The particles and pits form a fairly regular hexagonal array and repeat at an average center to center distance of 150–155 Å. Notice that the junctional membranes are curved, appearing convex on face E (Fig. 20) and concave on face P (Fig. 21). This is the most common type of junction in uncoupled cells and is similar to isolated, PTA-stained junctions (see Fig. 2, *inset*).

Published August 1, 1976

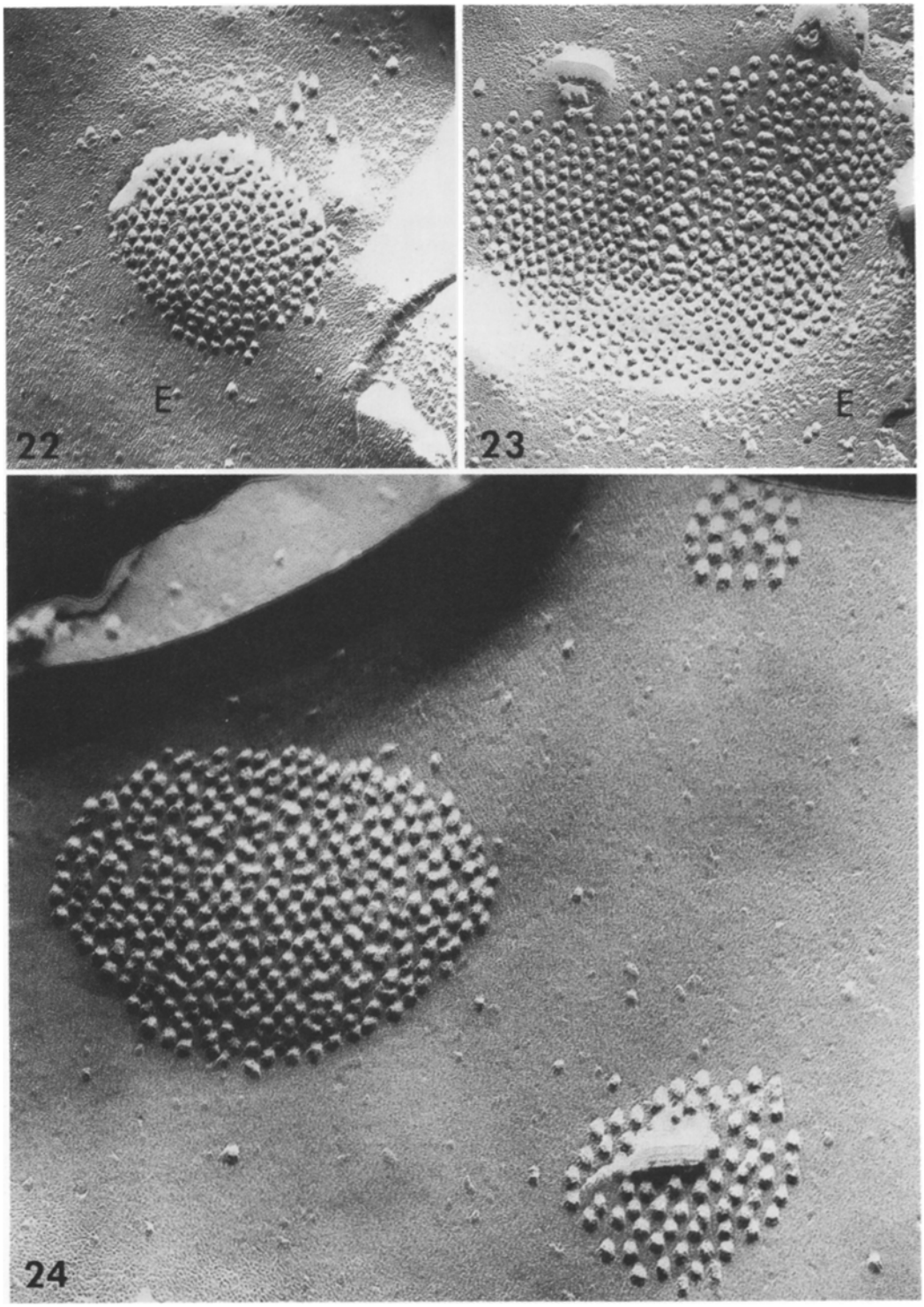

Published August 1, 1976

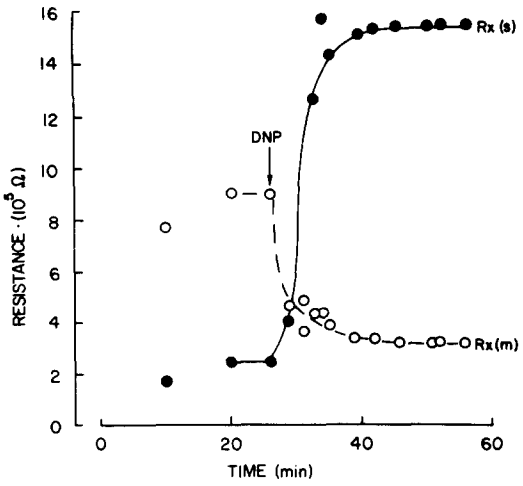

FIGURE 25 Time course of septal resistance $R_{x(s)}$ (filled circles), and membrane resistance $R_{x(m)}$ (open circles) during treatment with DNP. Notice the significant increase in $R_{x(s)}$ which reaches a plateau in ~10 min, and the simultaneous drop in $R_{x(m)}$.

the coupling resistance falls to near its prefixation values. The possibility that the recovery is due to the formation of new pathways between cells, as large holes through the junctions (7, 8), is unlikely because in this case one would expect a decrease of the junctional resistance below the control values. Furthermore, holes in the junctional membranes have never been seen in our freeze-fracture preparations of glutaraldehyde-fixed ganglia, which indicates that the ruptures in the junctional membranes, seen in sections, result probably from later treatment such as osmication and/or dehydration.

The mechanisms involved in the structural changes associated with uncoupling are still obscure. Calcium could bind to specific intracellular sites, causing conformational changes in particle protein. Changes in particle charges and/or their hydrophobicity may then result in aggregation. Other hypotheses could involve a reaction between calcium and specific lipid groups. Alternatively, calcium could activate a hypothetical contractile mechanism, causing both particle aggregation and conformational changes. The aggregation of the particles could produce a displacement of interparticle membrane components. Such components are likely to be lipids in a bilayer (19, 20, 33); therefore, because of the fluid nature of membrane bilayers (49), one may expect the aggregation and disaggregation of the particles to produce a translational flow of lipids towards and from, respectively, the perijunctional membrane regions.

The structural changes described here are not confined to crayfish axons and are probably typical of a general phenomenon. The gap junctions between mucous cells of rat stomach normally have particles irregularly packed at an average center to center distance of 95–100 Å. After treatment with DNP or anoxia, the particles aggregate more tightly to form regular hexagonal arrays with an average center to center distance of ~85 Å (35, 36).

In conclusion, a significant decrease in ionic permeability of crayfish gap junctions is paralleled by a change in the structure of the junctions. The structural changes are characterized by a tighter and more regular aggregation of the intramembrane particles, and a decrease in the overall width of the junction and in the thickness of the extracellular gap. Preliminary data indicate also a decrease in particle diameter. Reversible changes in permeability are paralleled by reversible changes in

FIGURES 22 and 23 Freeze-fracture replicas of junctions with particle periodicity of 150–155 Å, from ganglia treated as described in the legend of Fig. 12. Most often, these junctions appear convex on face E (Figs. 12, 20, 22). Concave E faces of junctions, however, are also seen (Fig. 23). The particle array of Fig. 23 is slightly disarranged in central areas. *E* = face E. × 123,600.

FIGURE 24 Freeze-fracture replica of junctions (Face E) from a ganglion treated as described in Fig. 12. The average center to center distance between adjacent particles is 150–155 Å in the junction on the left, ~200 Å in the two small junctions on the right. The presence of different types of junctions closely grouped in the same region of a cell is not a frequent occurrence. These cases provide useful specimens for measuring the size of the particles, since replica thickness and contamination are presumably the same. Measurements of the average diameter of the particles, normal to the direction of shadowing, give values of 121 ± 12.5 Å for the particles of the left junction, 152 ± 9.7 Å for the two right junctions (± indicates the standard deviation. $P = < 0.0001$). × 177,000.

Published August 1, 1976

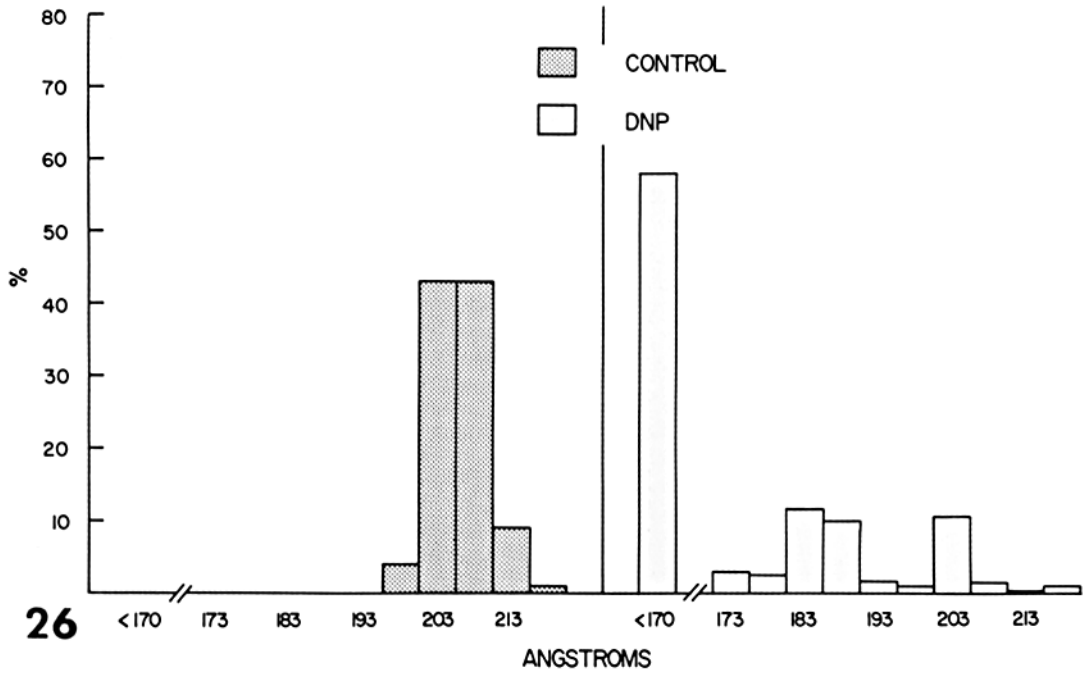

FIGURE 26 Histogram of frequencies (in percentiles) of center to center distances between adjacent beads measured on cross-sectional profiles of junctional membranes at the septa where the intracellular recordings were made. Notice that in controls 86% of the profiles show a particle periodicity of 200–210 Å, while after DNP more than 58% have a periodicity of <170 Å. A total length of 31.67 μm of cross-sectional profiles was measured (control = 7.89 μm; DNP = 23.78 μm).

FIGURE 27 Cross-sectional profile of a junction from a septum between lateral giant fibers treated with DNP. The septum was fixed in an uncoupled condition, i.e. after $R_{x(s)}$ reached a plateau (see Fig. 25). Most of the junctional profile (right of arrows) does not show particle images. In these regions, the overall width of the junction is ~180 Å, the gap measures 20–30 Å and the junction is not associated with regular layers of vesicles. On the left of the arrows, the junction is similar to controls (see Fig. 5), i.e. the average center to center distance between adjacent beads is 207 Å. Junctional and gap thickness are as in controls, and 400–700 Å vesicles lie close to either side of the junction. × 61,300.

FIGURE 28 Freeze-fracture of junctions (Face E) from a ganglion treated with DNP and fixed in uncoupled condition (see Fig. 25). All the junctions display hexagonally packed particles at an average center to center distance of 150–155 Å. Notice that most junctions are curved as similar junctions from EDTA-VH-treated ganglia (see Figs. 12, 20, 21–24), and nonjunctional membrane regions are wavy. The inset is a histogram of frequencies (in percentiles) of average particle periodicities in freeze-fractured control and DNP-treated junctions. Notice that in controls 83% of the junctions have particles at a center to center distance greater than 180 Å, while after DNP 74% have particles at a distance of 140–159 Å. 135 junctions were measured (control = 81; DNP = 54). × 57,000.

Published August 1, 1976

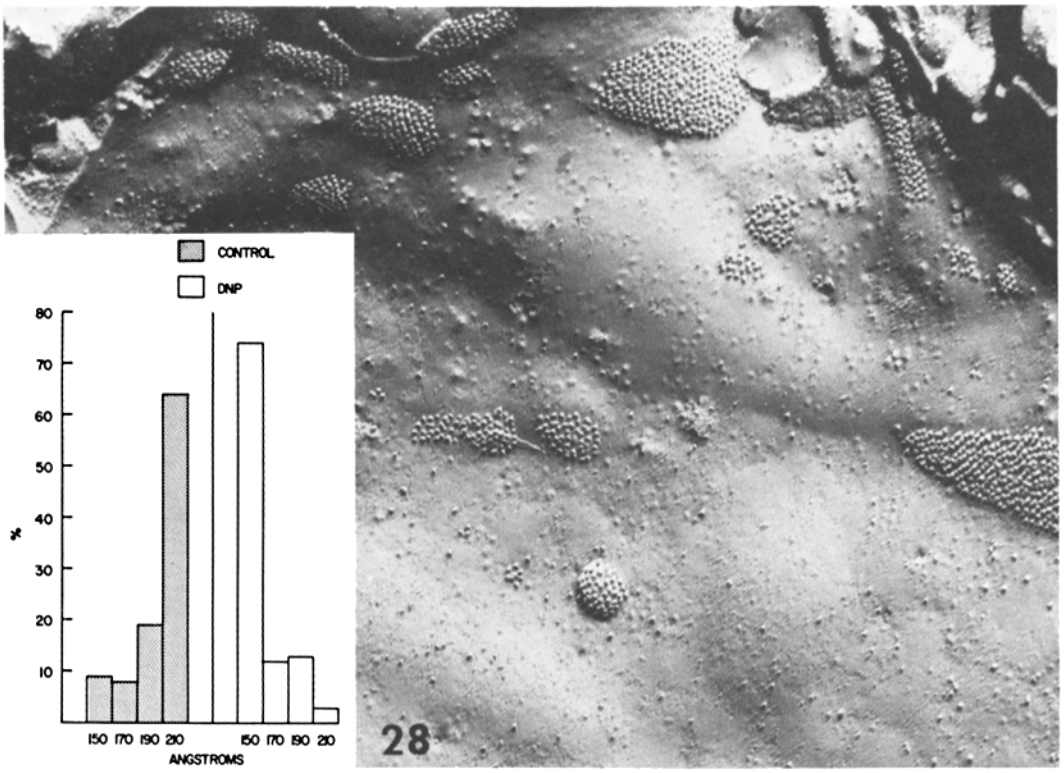

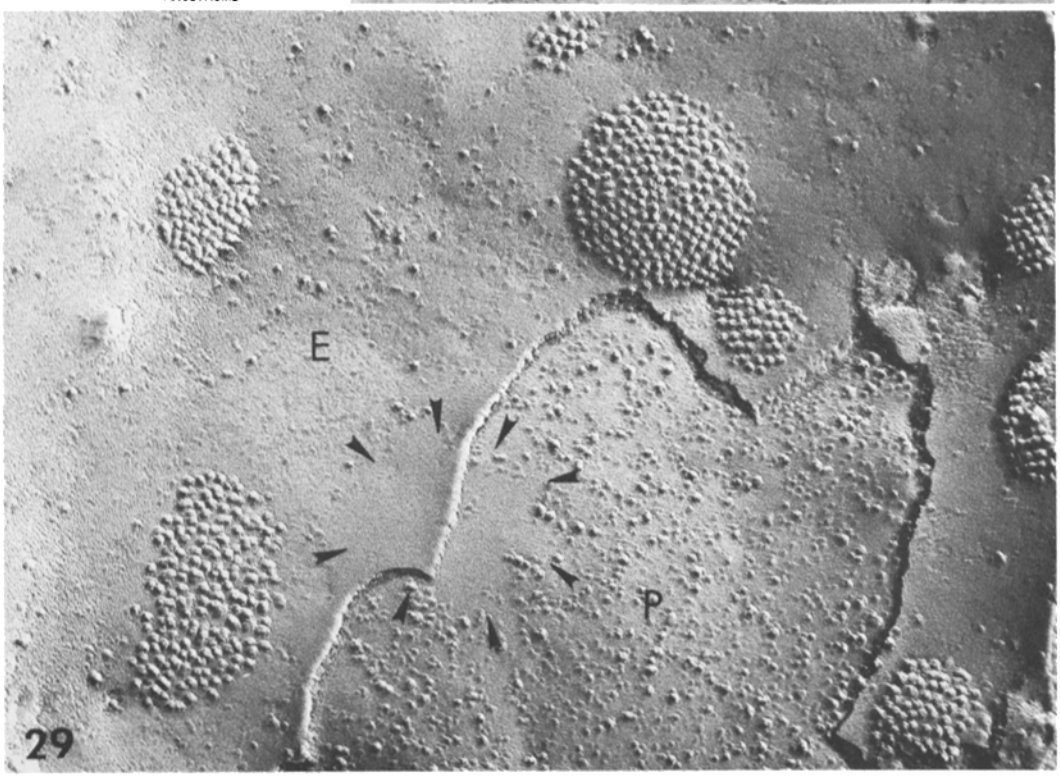

FIGURE 29 Freeze-fracture replica of junctions (Face E) from a ganglion treated with DNP and fixed in an uncoupled condition (see Fig. 25). As in Fig. 28, in all junctions the particles are at an average center to center distance of 150–155 Å. The random intramembrane particles show a tendency to aggregate. Limited by the arrowheads is a smooth, particle-free area. Notice that the smooth area in one cell (face E) (*E*) appears to match an equally smooth area in the adjacent cell (face P) (*P*). × 100,000.

structure. Both the decrease in permeability and the structural changes at the gap junctions are likely to be triggered by a reaction between Ca^{++} and specific Ca^{++}-binding sites at intracellular components of the junctional membranes. We suggest as a hypothesis that changes in permeability are caused by conformational changes in some components of the intramembrane particles at the gap junctions.

The authors wish to thank Mrs. Lillian Peracchia for her technical assistance.

This research was supported by grants from the National Institutes of Health (1 R01 GM20113 and 1 P01 NS10981).

Received for publication 3 December 1975, and in revised form 17 March 1976.

BIBLIOGRAPHY

1. ALMERS, W. 1972. Potassium conductance changes in skeletal muscle and the potassium concentration in the transverse tubules. *J. Physiol. (Lond.).* **225:**33-56.
2. ASADA, Y., and M. V. L. BENNETT. 1971. Experimental alteration of coupling resistance at an electrotonic synapse. *J. Cell Biol.* **49:**159-172.
3. ASADA, Y., G. D. PAPPAS, and M. V. L. BENNETT. 1967. Alteration of resistance at an electrotonic junction and morphological correlates. *Fed. Proc.* **26:**330.
4. BAKER, P. F., M. P. BLAUSTEIN, A. L. HODGKIN, and R. A. STEINHARDT. 1969. The influence of calcium on sodium efflux in squid axons. *J. Physiol. (Lond.).* **200:**431-458.
5. BAKER, P. F., A. L. HODGKIN, and E. B. RIDGWAY. 1971. Depolarization and calcium entry in squid giant axons. *J. Physiol. (Lond.).* **218:**709-755.
6. BENNETT, M. V. L. 1966. Physiology of electronic junctions. Biological Membranes: recent progress. Ann. N. Y. Acad. Sci. **137:**509-539.
7. BENNETT, M. V. L. 1973. Function of electrotonic junctions in embryonic and adult tissues. *Fed. Proc.* **32:**65-75.
8. BENNETT, M. V. L. 1973. Permeability and structure of electrotonic junctions and intercellular movements of tracers. *In* Intracellular Staining in Neurobiology. S. B. Kater and C. Nicholson, editor. Springer-Verlag, New York. 115-133.
9. BLAUSTEIN, M. P., and A. L. HODGKIN. 1969. The effects of cyanide on the efflux of calcium from squid axons. *J. Physiol. (Lond.).* **200:**497-527.
10. BRANTON, D., S. BULLIVANT, N. B. GILULA, M. J. KARNOVSKY, H. MOOR, K. MÜHLETHALER, D. H. NORTHCOTE, L. PACKER, B. SATIR, V. SPETH, L. A. STAEHELIN, R. L. STEERE, and R. S. WEINSTEIN. 1975. Freeze-etching nomenclature. *Science (Wash. D. C.).* **190:**54-56.
11. BULLIVANT, S., and W. R. LOEWENSTEIN. 1968. Structure of coupled and uncoupled cell junctions. *J. Cell Biol.* **37:**621-632.
12. CARAFOLI, E. 1967. In vivo effect of uncoupling agents on the incorporation of calcium and strontium into mitochondria and other subcellular fractions of rat liver. *J. Gen. Physiol.* **50:**1849-1864.
13. CARAFOLI, E., R. TIOZZO, G. LUGLI, F. CROVETTI, and C. KRATZING. 1974. The release of calcium from heart mitochondria by sodium. *J. Mol. Cell. Cardiol.* **6:**361-378.
14. DEMELLO, W. C. 1975. Effects of intracellular injection of calcium and strontium on cell communication in heart. *J. Physiol. (Lond.).* **250:**231-245.
15. DEWEY, M. M., and L. BARR. 1962. Intercellular connection between smooth muscle cells: the nexus. *Science (Wash. D. C.).* **137:**670-672.
16. DRAHOTA, Z., E. CARAFOLI, C. S. ROSSI, R. L. GAMBLE, and A. L. LEHNINGER. 1965. The steady state maintenance of accumulated Ca^{++} in rat liver mitochondria. *J. Biol. Chem.* **240:**2712-2720.
17. GAGE, P. W., and R. S. EISENBERG. 1969. Capacitance of the surface and transverse tubular membrane of frog sartorius muscle fibers. *J. Gen. Physiol.* **53:**265-278.
18. GREENAWALT, J. W., C. S. ROSSI, and A. L. LEHNINGER. 1964. Effect of active accumulation of calcium and phosphate ions on the structure of rat liver mitochondria. *J. Cell Biol.* **23:**21-38.
19. GOODENOUGH, D. A., D. L. D. CASPAR, L. MAKOWSKI, and W. C. PHILLIPS. 1974. X-ray diffraction of isolated gap junctions. *J. Cell Biol.* **63**(2, Pt. 2)**:** 115 a (Abstr.).
20. GOODENOUGH, D. A., and W. STOECKENIUS. 1972. The isolation of mouse hepatocyte gap junctions. Preliminary chemical characterization and X-ray diffraction. *J. Cell Biol.* **54:**646-656.
21. HODGKIN, A. L., and R. D. KEYNES. 1957. Movements of labelled calcium in squid giant axons. *J. Physiol. (Lond.).* **138:**253-281.
22. KEETER, J. S., DESCHÊNES, M., PAPPAS, G. D., and M. V. L. BENNETT. 1974. Fine structure and permeability of a rectifying electrotonic synapse. *Biol. Bull. (Woods Hole).* **147:**485-486.
23. LOEWENSTEIN, W. R. 1967. Cell surface membranes in close contact. Role of calcium and magnesium ions. *J. Colloid. Sci.* **25:**34-46.
24. LOEWENSTEIN, W. R., M. NAKAS, and S. J. SOCOLAR. 1967. Junctional membrane uncoupling: permeability transformations at a cell membrane junction. *J. Gen. Physiol.* **50:**1865-1891.
25. LUXORO, M., and E. YAÑES. 1968. Permeability of the giant axon of *Dosidicus gigas* to calcium ions. *J. Gen. Physiol.* **51:**115S-122S.
26. NAKAS, M., S. HIGASHINO, and W. R. LOEWENSTEIN. 1966. Uncoupling of an epithelial cell mem-

brane junction by calcium-ion removal. *Science (Wash. D. C.).* **151:**89–91.

27. OLIVEIRA-CASTRO, G. M., and W. R. LOEWENSTEIN. 1971. Junctional membrane permeability—effects of divalent cations. *J. Membr. Biol.* **5:** 51–77.
28. PAPPAS, G. D., Y. ASADA, and M. V. L. BENNETT. 1967. Morphological and physiological changes in junctional sites of crayfish septate axons. *Anat. Rec.* **157:**297.
29. PAPPAS, G. D., Y. ASADA, and M. V. L. BENNETT. 1971. Morphological correlates of increased coupling resistance at an electrotonic synapse. *J. Cell Biol.* **49:**173–188.
30. PAYTON, B. W., M. V. L. BENNETT, and G. D. PAPPAS. 1969. Temperature-dependence of resistance at an electrotonic synapse. *Science (Wash. D. C.).* **165:**594–597.
31. PERACCHIA, C. 1972. Gap junctions: new structural details. *J. Cell Biol.* **55:**202a.
32. PERACCHIA, C. 1973. Low resistance junctions in crayfish. I. Two arrays of globules in junctional membranes. *J. Cell Biol.* **57:**54–65.
33. PERACCHIA, C. 1973. Low resistance junctions in crayfish. II. Structural details and further evidence for intercellular channels by freeze-fracture and negative staining. *J. Cell Biol.* **57:**66–76.
34. PERACCHIA, C. 1974. Excitable membrane ultrastructure. I. Freeze-fracture of crayfish axons. *J. Cell Biol.* **61:**107–122.
35. PERACCHIA, C. 1974. A structure-function correlation in gap junctions of crayfish. Abstracts of the 8th International Congress on Electron Microscopy. J. V. Sanders and D. J. Goodchild, editors. The Australian Academy of Sciences, Canberra A. C. T. Australia. Vol. II. 226–227.
36. PERACCHIA, C., and A. F. DULHUNTY. 1974. Gap junctions: Structural changes associated with changes in permeability. *J. Cell Biol.* **63**(2, Pt. 2):263 a (Abstr.).
37. PERACCHIA, C., and B. S. MITTLER. 1972. Fixation by means of glutaraldehyde-hydrogen peroxide reaction products. *J. Cell Biol.* **53:**234–238.
38. POLITOFF, A., and G. D. PAPPAS. 1972. Mechanisms of increase in coupling resistance at electrotonic synapses of the crayfish septate axons. *Anat. Rec.* **172:**384–385.
39. POLITOFF, A. L., S. J. SOCOLAR, and W. R. LOEWENSTEIN. 1969. Permeability of a cell membrane junction: Dependence on energy metabolism. *J. Gen. Physiol.* **53:**498–515.
40. REVEL, J. P. 1968. Studies on the fine structure of intercellular junctions. Proceedings of the 26th Meeting of the Electron Microscopy Society of America. Claitor's Publishing Division, Baton Rouge, La. 40.
41. REVEL, J. P., and M. J. KARNOVSKY. 1967. Hexagonal array of subunits in intercellular junctions of the mouse heart and liver. *J. Cell Biol.* **33:**C7–C12.
42. ROBERTSON, J. D. 1963. The occurrence of a subunit pattern in the unit membranes of club endings in Mauthner cell synapses in goldfish brains. *J. Cell Biol.* **19:**201–222.
43. ROSE, B. 1971. Intercellular communication and some structural aspects of membrane junctions in a simple cell system. *J. Membr. Biol.* **5:**1–19.
44. ROSE, B., and W. R. LOEWENSTEIN. 1971. Junctional membrane permeability. Depression by substitution of Li for extracellular Na, and by long-term lack of Ca and Mg; Restoration by cell repolarization. *J. Membr. Biol.* **5:**20–50.
45. ROSE, B., and W. R. LOEWENSTEIN. 1974. Cytoplasmic free calcium and intercellular coupling. *Fed. Proc.* **33:**1340.
46. ROSE, B., and W. R. LOEWENSTEIN. 1975. Permeability of cell junction depends on local cytoplasmic calcium activity. *Nature (Lond.).* **254:**250–252.
47. SATO, T. 1968. A modified method for lead staining of thin sections. *J. Electron Microsc.* **17:**158–159.
48. SHIMOMURA, O., F. H. JOHNSON, and Y. SAIGA. 1962. Extraction, purification and properties of Aequorin, a bioluminescent protein from the luminous hydromedusan, Aequorea. *J. Cell. Comp. Physiol.* **59:**223–239.
49. SINGER, S. J., and G. L. NICHOLSON. 1972. The fluid mosaic model of the structure of cell membranes. *Science (Wash. D. C.).* **175:**720–731.
50. STAEHELIN, L. A. 1974. Structure and function of intercellular junctions. *Int. Rev. Cytol.* **39:**191–283.
51. VAN HARREVELD, A. 1936. A physiological solution for fresh water crustaceans. *Proc. Soc. Exp. Biol. Med.* **34:**428–432.
52. VASINGTON, F. D., and J. V. MURPHY. 1962. Ca^{++} uptake by rat kidney mitochondria and its dependence on respiration and phosphorylation. *J. Biol. Chem.* **237:**2670–2677.
53. WATANABE, A., and H. GRUNDFEST. 1961. Impulse propagation at the septal and commissural junctions of crayfish lateral giant axons. *J. Gen. Physiol.* **45:**267–308.
54. ZAMPIGHI, G., and J. D. ROBERTSON. 1973. Fine structure of the synaptic discs separated from the goldfish medulla oblongata. *J. Cell Biol.* **56:**92–105.